Temperature-dependent Microstructural Evolution of Ti_2AlN Thin Films Deposited by Reactive Magnetron Sputtering

Zheng ZHANG,[†] Hongmei JIN,[‡] Jianwei CHAI,[†] Jisheng PAN,[†] Hwee Leng SENG,[†] Glen Tai Wei GOH,[†] Lai Mun WONG,[†] Michael B. SULLIVAN,[‡] and Shi Jie WANG[†]***

[†] Institute of Materials Research and Engineering, A*STAR (Agency for Science, Technology and Research), #08-03, Innovis, 2 Fusionopolis Way, 138634, Singapore.

[‡] Institute of High Performance Computing, A*STAR (Agency for Science, Technology and Research), 1 Fusionopolis Way, Connexis, 138632, Singapore.

Corresponding Authors:

*Tel.: +65-64191332

*Fax: +65-64632536

*E-mail address: jinhm@ihpc.a-star.edu.sg

**Tel.: +65-64168953

**Fax: +65-68720785

**E-mail address: sj-wang@imre.a-star.edu.sg

ABSTRACT

Ti_2AlN MAX phase thin films have been deposited on MgO (111) substrates between 500 and 750 ^oC using DC reactive magnetron sputtering of a Ti_2Al compound target in a mixed N_2/Ar plasma. The composition, crystallinity, morphology and hardness of the thin films have been characterized by X-ray photoelectron spectroscopy, X-ray diffraction, atomic force microscopy and nano-indentation, respectively. The film initially forms a mixture of Ti, Al and (Ti,Al)N cubic solid solution at 500 ^oC, and nucleates into polycrystalline Ti_2AlN MAX phases at 600 ^oC. Its crystallinity is further improved with an increase in the substrate temperature. At 750 ^oC, single crystalline Ti_2AlN (0002) thin film is formed having characteristic layered hexagonal surface morphology, high hardness, high Young's modulus and low electrical resistivity. The mechanism behind the evolution of the microstructure with growth temperature is discussed in terms of surface energies, lattice mismatch and enhanced adatom diffusion at high growth temperatures.

Keywords: Ti_2AlN; MAX Phase; Sputtering; Surface Diffusion; Surface Energy; Temperature-dependent.

1. Introduction

The $M_{n+1}AX_n$ (n = 1-3) or MAX phase materials are a group of about 60 nanolaminate ternary carbides and/or nitrides (X = carbon or nitrogen) of transition metals (M), which are constructed by vertically repeating two $M_{n+1}X_n$ layers intercalated by one layer of a group 12-16 element (A) in between [1]. After their initial discovery in 1960s, this group of materials has regained significant attentions since mid-1990s upon the discovery of their unique combination of both ceramic and metallic properties. On one hand, like ceramics, MAX phase materials have high melting points and high temperature oxidation resistance. On the other hand, like metals, MAX phase materials have good electrical and thermal conductivity, high ductility, easy machinability, superior thermal shock resistance and damage tolerance [2]. The distinctive combination of these properties stems from co-existence of the strong covalent-ionic M-X bonds and the weak metallic M-A bonds inside the layered hexagonal structures of MAX materials [1-3]. Their exceptional properties have led to the exploration of a variety of applications including high temperature protective coatings on turbine blades [4], radiation-tolerant cladding material for next generation nuclear power plants [5], and a candidate as Ohmic contact to SiC [6].

Relatively phase-pure MAX phase materials were initially synthesized by hot isostatic pressing (HIP) of the respective starting powders (i.e., MX + AX, or MX + A, or M + A + X) under high pressure and high temperature [1]. Some well-studied MAX phase materials include Ti_3SiC_2, Ti_2AlC and Ti_4AlN_3. Although there are presence of other minority phases as impurities in the final products, this HIP fabrication method has offered the first hand opportunity to characterize these MAX phase materials' macroscopic properties including density, electrical resistivity, heat capacities, hardness, Young's modulus and oxidation resistance, etc [1]. Recently thin film deposition technique primarily using sputtering has been employed to grow several

carbide-based MAX phase materials including Ti_3SiC_2 [7,8], Ti_2AlC [9], Cr_2AlC [10,11], Cr_2GeC [12], Ti_4SiC_3 [13], Ti_3GeC_2 [13], Ti_2GeC [13], Ti_2SnC [13], V_2AlC [14] and one nitride-based MAX phase material, Ti_2AlN [3,15-22]. The setups in these sputtering chambers can be pretty versatile to cater for different MAX phase material systems: from individual elemental targets to compound targets and from pure Ar plasma to a mixture of Ar/N_2 plasma. The sputtering technique not only offers the possibility to grow single crystalline MAX phase thin films so that their microscopic properties such as atomic structure and lattice arrangement can be determined, but also offers the opportunity to engineer the stoichiometry of the thin films and to grow multi-layer structures.

Single crystalline Ti_2AlN thin films have recently been grown epitaxially on single-crystal MgO(111) and Al_2O_3(0001) substrates through ultra-high-vacuum (UHV) DC magnetron sputtering [3,15-22]. While carbon in the carbide-based MAX phase material is introduced from sputtering a graphite or C_{60} solid targets, nitrogen in nitride-based Ti_2AlN MAX phase material is mainly introduced from the gaseous nitrogen in the mixed Ar/N_2 plasma. Hence, considerable attentions have been focused to establish a N_2 partial pressure window so that the resultant thin film can achieve an appropriate N concentration in order for the Ti_2AlN MAX phase to nucleate and grow [18,19]. The results showed that that nitrogen-deficient conditions typically yield thin films with mixture of inverse perovskite Ti_3AlN phase and intermetallic TiAl and Ti_3Al phases, while nitrogen-rich conditions yield the binary nitride TiN and/or the Ti_2AlN [18,19]. By comparison, little efforts have been devoted to understand the influence of the substrate temperature on the microstructure of the resulting Ti-Al-N thin films [21]. Substrate temperature has been reported to exercise significant effects during growth of several carbide-based MAX phase thin films such as Ti_3SiC_2 [7], Ti_2AlC [9], Cr_2GeC [12], Cr_2AlC [11] and V_2GeC [14].

Although the exact influences varies among different MAX phase materials, two common observations are that high temperature (≥ 370 ºC) is required for the nucleation of MAX phase materials due to their large unit cell sizes (c ~13 Å for M_2AX phase, c ~ 18 Å for M_3AX_2 phase and c ~ 23-24 Å for M_4AX_3 phase) and that an increase in deposition temperature leads to a greater loss of A elements (like Al, Sn, Ge, etc) due to evaporation from the thin films because of their high vapor pressures [2]. For Ti_2AlN MAX phase thin film, a growth condition (which yields an amorphous Ti-Al-N thin film in a ratio of Ti : Al : N = 4 : 1 : 3 at room temperature) has led to the formation of a layered polycrystalline $Ti_{n+1}AlN_n$ structure which maintained an overall 4 : 1 : 3 stoichiometry but had both horizontal and nearly perpendicular orientations at 600 ºC. By increasing the deposition temperature to 675 ºC and above, the same growth condition resulted in the formation a mixture of TiN and Ti_2AlN instead [21]. Beckers *et al* attributed the reason behind different phases with a change in deposition temperature to severe loss of Al to vacuum at higher temperatures [21]. By comparing three independent studies, it is perplexed but interesting to observe that while basal planes of Ti_2AlN single crystalline films are grown on MgO (111) substrates at 830 ºC [15] and 750 ºC [20] with an epitaxial relationship of $Ti_2AlN\{0001\}<\bar{1}2\bar{1}0>//MgO\{111\}<110>$, non-basal planes of Ti_2AlN single crystalline film are developed on MgO (111) substrate by lowering substrate temperature further to 690 ºC, which results in an epitaxial relationship of $Ti_2AlN\{10\bar{1}2\}<\bar{1}2\bar{1}0>//MgO\{111\}<110>$ [17]. Beckers *et al* explained the non-basal plane growth to be caused by different interfacial adaptation due to kinetic restrictions of incoming atoms [17]. Hence, the growth temperature plays a significant role in the formation of high quality Ti_2AlN thin film but its contribution is yet to be clearly understood.

Therefore, in this work, we investigate the effect of substrate temperature on the

microstructure of resulting Ti-Al-N thin film deposited from 500 to 750 ºC *in-situ* by X-ray photoelectron spectroscopy (XPS) and *ex-situ* by X-ray diffraction (XRD), atomic force microscopy (AFM) and nano-indentation. We will show that polycrystalline Ti_2AlN MAX phase starts to nucleate at as low as 600 ºC. Its crystallinity further improves at 700 and 720 ºC until it transforms into single crystalline phase at 750 ºC. The mechanism behind the evolution of the microstructure with temperature will be discussed by considering various factors including surface energy, lattice mismatch and enhanced adatom diffusion at high growth temperatures.

2. Experimental methods

Single crystalline MgO (111) wafers are chosen as substrates to deposit Ti_2AlN thin films, because MgO (111) plane has a very small lattice mismatch of only 0.57 % with Ti_2AlN (0002) plane and therefore is promising to facilitate the growth of epitaxial Ti_2AlN (0002) single crystalline thin film. The MgO (111) wafer were cleaned ultrasonically in acetone, isopropanol and de-ionized water before being introduced in the growth chamber with a base pressure of 5.0×10^{-9} mbar. They were further degassed at 800 ºC for 1 hour and then cleaned by N_2 atomic source for 30 minutes to remove surface carbonaceous contamination. A three inch Ti_2Al alloy target (99.99 % purity) was used for deposition using direct-current (DC) magnetron sputtering at a power of 90 W. While the partial pressures of Ar and N_2 during deposition were fixed at 3.2×10^{-3} and 6.0×10^{-5} mbar, respectively, the substrate temperature was monitored by pyrometer and was set at 500, 600, 700, 720 and 750 ºC at different batches in order to study the effect of substrate temperature. After deposition, the samples were transferred to the analysis chamber of VG ESCALAB 220i-XL XPS *in-situ* without exposing to air. A monochromatic Al *Kα* (1486.7 eV) X-ray with a diameter of 700 μm is employed while the photoelectrons are collected at a

normal take-off angle (with respect to surface plane). After one hour deposition, the thicknesses of Ti_2AlN thin films were measured to be around 300 nm by a surface profiler. The crystalline structures of thin films were investigated using Bruker general area detector diffraction system (GADDS) XRD operated at a voltage of 40 kV and a current of 40 mA (Cu Kα X-ray, λ=1.54Å), while the surface morphology of the films was examined by Bruker Dimension ICON AFM. The hardness and Young's modulus of the films were determined from a MTS Nano Indenter XP® using a continuous stiffness measurement (CSM) technique with a Berkovich indenter (three-faced pyramid diamond). During the indentation test, the indenter was pressed from the surface to 300 nm deep into the composite film with a constant strain rate (0.05 s^{-1}), which was loaded on the samples in order to avoid strain-hardening effect on the measurements. This method allows stiffness of the film to be recorded continuously along the indentation depth. As such, modulus and hardness can be derived and their profiles can be plotted against displacement into surface [23]. The hardness and modulus values at the plateau within 10% of the total film thickness, which is 30 nm from the surface, were recorded as films' properties to ensure that the values actually correspond to the films' properties and do not influence by substrate or surface effects. An average value based on ten indentations measurement at 100 μm apart on the Ti_2AlN thin film was reported for each temperature. It it worth noting that the measured modulus is a reduced modulus (E_r), which can be converted to the Young's modulus of the test specimen (E_s) through the following equation:

$$\frac{1}{E_r} = \frac{1-v_i^2}{E_i} + \frac{1-v_s^2}{E_s} \quad (1)$$

where E_i and ν_i are Young's modulus (1140 GPa) and Poisson's ratio (0.07) for the diamond indenter tip, ν_s is the Poisson's ratio (0.3) for the samples.

3. Results

The XPS spectra of Ti 2p, Al 2p, N 1s, valence band (VB), Mg 1s and O 1s of the resulting Ti-Al-N thin films at different growth temperatures of 500, 600, 700, 720 and 750 ºC were taken immediately after growth *in-situ* without exposing to air and are shown in Fig. 1. At 500 ºC, it can be seen that there were two components within Ti $2p_{3/2}$ peak after peak fitting: one at 454.4 eV and the other one at 455.0 eV. They represent a metallic Ti and TiN, respectively. A small component at 457.8 eV is associated with Ti 2p shake-up satellite in TiN [24]. There are two components inside Al 2p peak as well: one at 72.6 eV representing metallic Al and the other at 74.5 eV representing AlN [25]. There are also two components inside N 1s peak: a strong one at 397.3 eV representing nitrides (TiN and AlN) and a weak one at 398.3 eV representing oxygen-containing nitrides (O-TiN or O-AlN). Hence, the XPS results suggest formation of a mixture of TiN and AlN together with excess metallic Ti and Al at 500 ºC.

From 600 to 750 ºC, only a single peak is detected in Ti $2p_{3/2}$ (454.4 eV at 600 ~ 720 ºC, 454.6 eV at 750 ºC), Al 2p (72.3 eV) and N 1s (397.5 eV) spectra, indicating a single chemical state for Ti, Al and N. It is worth to note that the binding energy (BE) of Ti $2p_{3/2}$ in these temperature region (600 ~ 750 ºC) is close but lower than that in TiN (455.1 eV), although the BE of N 1s in this region is the same as that in TiN (397.4 eV) [26]. BE of Al 2p is lower than those in AlN (74.4 eV) and even metallic Al (72.9 eV) but higher than that in TiAl alloy (71.4 eV) [25,27]. In addition, there is clearly an increase in the intensity in the region of -0.4 and -1.6 eV in the VB (Fig. 1(d)) for samples deposited between 600 and 750 ºC. As discussed previously, the BE of Ti $2p_{3/2}$ and Al 2p at 454.6 and 72.3 eV as well as the unique shape of the VB in the region of -0.4 and -1.6 eV are actually characteristics of Ti_2AlN MAX phase and can be used to determine its formation [20]. Therefore, XPS result indicates that Ti_2AlN MAX phase

is formed when the substrate temperature is raised to 600 ºC and above. Meanwhile, no Mg 1s signals were detected while O 1s intensity remained fairly constant, implying that there is no diffusion of MgO from substrate to the surface.

The composition of N (N %) decreased significantly from 42.3 % to 24.2 % (Fig. 1(f)), when the temperature increased from 500 to 600 ºC. At the same time, Ti % and Al % increased from 22.5 % to 37.1 % and from 35.2 % to 38.7 %, respectively. At 700 ºC, Al % started to decrease from 38.7 % to 36.3 %, while both Ti % and N % increased from 37.1 % to 38.8 % and from 24.2 % to 24.9 %.When the temperature was raised to 720 ºC, Al further decreased to 29.3 % (vs 42.2 % Ti and 28.5 % N) and it decreased again to only 14.8 % (vs 45.2 % Ti and 40.0 % N) when the temperature was increased to 750 ºC.

The crystalline structures of the resulting films between 500 and 750 ºC were examined using Bruker GADDS XRD, which employs an area detector to capture the diffraction patterns over a 2θ width of 36 º per frame. Two consecutive frames covering 2θ ranges from 10 ~ 46 º and 41 ~ 77 º were captured and subsequently integrated over 2θ and Chi (Ψ) to obtain a 2θ range of 10 ~ 77 º. The first frames covering diffraction patterns in the 2θ ranges of 10 ~ 46 º (from right to left direction) are shown in Fig. 2(a-e). After capturing the respective second frame covering 2θ ranges of 41 ~ 77 º and integrating these two frames, the complete XRD spectra covering a range of 10 ~ 77 º is shown in Fig. 2(f). It can be seen from Fig. 2(f) that the crystalline phase in the thin film deposited at 500 ºC was mainly composed of (Ti,Al)N cubic solid solution [28]. Metallic Ti and Al phases, which are identified in Ti 2p and Al 2p high resolution XPS spectra, might be amorphous or in nano-crystallite shape (Fig. 3(a)) and hence are not detected by XRD. The single dot at Fig. 2(a) represents the diffraction spot from single crystal MgO (111) plane at 2θ of 37.1 º, while two weak diffraction rings at 36.8 º and 42.8 º

representing (Ti,Al)N (111) and (Ti,Al)N (200) planes can be vaguely identified. One advantage of using an area detector in XRD is the capability to qualitatively determine the crystalline quality by looking at the diffraction pattern: a single diffraction spot, a continuous diffraction ring and a broken diffraction ring indicate single crystalline, polycrystalline and highly textured polycrystalline phases, respectively.

At 600 ºC, two diffraction rings at 34.7 and 40.1 º representing Ti_2AlN (100) and Ti_2AlN (103) phases can be seen in the first frame captured by the area detector (Fig. 2(b)). After integration with second frame, it can be seen that the phases at 600 ºC includes intense planes such as (103), (116) and (106), as well as some weak planes including (100), (104), (106), (110) and (107). In agreement with the XPS results, Ti_2AlN phase does form at 600 ºC, and it is a polycrystalline phase as shown by XRD results.

At 700 ºC, two extra diffraction spots at 13.0 and 39.2 º appeared (Fig. 2(c)) besides the two diffraction rings at 34.7 and 40.1 º which were observed earlier at 600 ºC. These two diffraction spots correspond to Ti_2AlN (002) and (004) planes, which imply formation of basal planes of Ti_2AlN at 700 ºC.

At 720 ºC, the diffraction ring at 40.1 º representing Ti_2AlN (103) plane observed at 600 and 700 ºC became four separated arcs which were distributed along the 2θ position of the same diffraction ring (Fig. 2(d)). This indicates that the Ti_2AlN (103) plane has become highly textured or ordered at 720 ºC. After peak integration, it was observed that the intensity of Ti_2AlN (004) plane increased significantly, while Ti_2AlN (116) plane decreased substantially.

At 750 ºC, only two diffraction spots at 13.0 and 39.2 º corresponding to Ti_2AlN (002) and (004) planes were observed (Fig. 2(e)), implying formation of single crystalline Ti_2AlN (002) phase at 750 ºC. By scanning the pole figures of Ti_2AlN $\{10\bar{1}3\}$ & $\{10\bar{1}1\}$ planes and

MgO {111} planes using PANalytical X'pert PRO XRD, the orientation relationship between the film and substrate has been determined to be Ti_2AlN (0002)[$\bar{1}2\bar{1}0$] // MgO (111)[011] as reported in our previous work [20].

With the development of the crystalline plane and the stacking direction between planes as a function of deposition temperature, the surface morphology and mechanical properties will likely change as a result. Therefore, surface morphology and mechanical properties of the Ti-Al-N thin films deposited between 500 and 750 ^oC were examined by AFM and nano-indentation, and the results are shown in Fig. 3 and Fig. 4, respectively.

The surface of the Ti-Al-N thin film at 500 ^oC was relatively flat and mainly consisted of circular domes having a diameter range of 50 ~ 100 nm (Fig. 3(a)). At 600 ^oC, the film became much rougher (Fig. 3(b)). A closer look at the 2 × 2 μm^2 image shows islands having a hint of triangle shape (marked by blue circle). The edge of the triangle consisted of several layers with a layer thickness of 28 - 50 nm. At 700 ^oC, the surface was still much undulated (Fig. 3(c)). However, the triangle islands grew in size which made them easily discernible even in a 5 × 5 μm^2 image. In the 2 × 2 μm^2 image, equilateral triangle islands can be clearly seen. At 720 ^oC, the surface has transformed into a wide-spread arrays of islands consisting of 2-5 layers with a layer thickness of 40 ~ 80 nm (Fig. 3(d)). Each array was either parallel to its neighbor array or forming an angle of 60 ^{o} / 120 ^{o} with its neighbor. Besides arrays of islands, flat areas marked by black circles can be seen. By measuring the line profiles across the islands and the flat areas (e.g, two lines marked in Fig. 3(d)), the islands can be found to sit on the flat area with an island height of 40 ~ 60 nm. At 750 ^oC, the surface has evolved into flat terraced morphology with a hint of hexagonal shape. Most of the step height was measured to be 1.4 ± 0.2 nm, close to lattice constant of 1.3614 nm in *c*-axis [1] of one unit cell of Ti_2AlN (0001). Thus, the morphology at

750 ºC revealed by AFM suggests a step-flow growth of single crystalline Ti_2AlN (0001) basal plane on MgO (111) substrate at 750 ºC.

The evolvement of hardness and Young's modulus of the Ti-Al-N films as a function of deposition temperature are measured by nano-indentation and are shown in Fig. 4. At 500 ºC, the film had a hardness of 8.8 ± 2.9 GPa and Young's modulus of 245.9 ± 72.2 GPa. Both two values are lowest compared to the readings at the other four deposition temperatures. Between 600 and 750 ºC where Ti_2AlN phase is formed, the Young's modulus remained roughly stable at 412.5 ± 45.6 GPa. However, the hardness increased linearly from 15.8 ± 2.6 GPa at 600 ºC to 26.5 ± 1.8 at 750 ºC, as the Ti_2AlN films developed from mixed polycrystalline phases to pure single crystalline phase.

4. Discussion

MAX phase materials typically have large *c*-axis parameters, i.e., >10 Å, which usually requires higher deposition temperature so that the adatoms can gain sufficiently high kinetic energy and mobility to diffuse and re-arrange themselves into the complex hexagonal structures comprised of large unit cells. Hence, the lowest formation temperatures reported for MAX phase so far are 370 ºC for Cr_2AlC [11] and 450 ºC for V_2GeC [14] thin films. For Ti_2AlN, a substrate temperature of 750 ~ 830 ºC [15,20] is required for basal plane growth of single-crystalline Ti_2AlN (0002) thin films on MgO (111) substrate, as lowering substrate temperature further to 690 ºC leads to non-basal plane growth of single-crystalline Ti_2AlN $(10\bar{1}2)$ thin film on MgO (111) substrate [17]. A substrate temperature of 450 ºC is not sufficient for Ti_2AlN MAX phase to nucleate, when Kim *et al* deposited Ti_2AlN thin film by sputtering a Ti_2AlN compound target [29]. Through the systematic investigation of the Ti-Al-N thin films deposited at different

temperatures in this work, it is clear by now that the nucleation of polycrystalline Ti_2AlN MAX phase can actually occur at as low as 600 ^oC. The crystallinity of Ti_2AlN MAX phase is improved with an increase in substrate temperature until the single crystalline Ti_2AlN MAX phase is achieved at 750 ^oC.

While an increase in substrate temperature improves the crystallinity of Ti_2AlN phase, it also leads to a significant decrease of Al % from 38.7 % at 600 ^oC to only 14.8 % at 750 ^oC (Fig. 1(f)). This is attributed to re-evaporation of Al from the surface due to its high vapor pressure. An increase in substrate temperature from 600 to 750 ^oC leads to a dramatic increase in Al's vapor pressure from 3.74×10^{-8} mbar to 3.06×10^{-5} mbar, which exaggerates the loss of Al from the surface of the growing film. Similarly, a decrease in Al % has been observed when the substrate temperature was increased during deposition of Ti_2AlC thin films using sputtering [9]. Nevertheless, the resulting Ti_2AlN thin film is still able to maintain its MAX phase structure despite losing part of Al atoms. The reason, shown by our recent density functional theory (DFT) calculation, is that the Ti_2AlN phase is able to maintain its structural stability even with loss of up to 20 % Al [30]. Such structural tolerance to Al deficiency is also shared by another MAX phase material, Ti_2AlC, which is also able to remain its structural stability after losing not more than 50 % of the Al atoms [31]. As a result, both Ti_2AlC and Ti_2AlN are subjected to investigation of radiation tolerance capability in order to explore their application as cladding material for future nuclear fuel [32-34]. Indeed, the calculation results have predicted both Ti_2AlC and Ti_2AlN to be the two most competent MAX phases in tolerating radiation damage [32], while experiments show that Ti_2AlN does withstand 100 keV Ar^{2+} ion irradiation [33] and 0.1 displacement per atom of neutron radiation [34].

Another interesting development with an increase of deposition temperature is the shift of

binding energy (BE) of Ti $2p_{3/2}$. Between 600 and 720 °C when polycrystalline Ti_2AlN MAX phase is formed, BE of Ti $2p_{3/2}$ stayed constant at 454.4 eV. However, it shifted to higher value of 454.6 eV, when the deposition temperature was raised to 750 °C. This can be explained by the Ti charge's re-distribution due to significant loss of Al at 750 °C. Our previous DFT calculation of charge transfer shows that in bulk Ti_2AlN, each Ti atom loses 1.23 electrons and two of them lose 2.46 electrons, with −1.75 and −0.71 electron transferred to N and Al atoms, respectively [20]. Due to the loss of Al, the electron charge which is supposed to transfer to Al atom will be re-distributed to a more electronegative atom, N, leading to higher electron loss from Ti, which is reflected as the shift of Ti $2p_{3/2}$ BE to a higher value. Another supporting evidence is the continual shift of Ti $2p_{3/2}$ BE to a higher value at 456.7 eV, after Al continues to lose from the Ti_2AlN thin film through desorption when the Ti_2AlN thin film is heated up in the ultra-high-vacuum chamber of XPS to 900 °C, where Al is decreased substantially to only ~4.3 % [35]. The electron gain of N from Ti before and after partial loss of Al from Ti_2AlN thin film is similar [35] and hence BE of N 1s does not show any significant changes.

The triangular morphology observed in Ti_2AlN thin films deposited between 600 and 720 °C is associated with formation of non-basal Ti_2AlN planes including (101), (103) and (116), etc (Fig. 2). Due to six-fold symmetry of Ti_2AlN hexagonal unit cell, {103} or $\{10\bar{1}3\}$ plane has six equal/symmetric counterparts by rotating 60 ° about the *c*-axis. If $\{10\bar{1}3\}$ planes are nucleated in such a way assuming that the Ti_2AlN unit cells are arranged vertically with respect to MgO (111) plane, intersecting of three $\{10\bar{1}3\}$ planes on a basal plane (i.e., a combination of $(10\bar{1}3)$, $(\bar{1}103)$ and $(0\bar{1}13)$ or a combination of $(1\bar{1}03)$, $(01\bar{1}3)$ and $(\bar{1}013)$) will form a tetrahedron, which truncated by a (0002) basal plane will turn into equilateral triangular top as imaged by AFM or SEM. Similarly, nucleation of other Ti_2AlN planes including (116), (101), etc, provided that the

Ti_2AlN unit cells are arranged upright will also lead to equilateral triangular surface morphology.

Tilted thin plates of other MAX phase materials including Ti_3SiC_2 [7], Cr_2AlC [11], Cr_2GeC [12], Ti_2SnC [13] and Ti_2AlC [36] have been reported, and are attributed to non-basal-plane growth of respective MAX phase thin films. Among them, the appearance of triangular islands is similarly observed during growth of Ti_2SnC (103) on Al_2O_3 (0001) at 720 ºC [13], Ti_2AlC (103) and (106) on Al_2O_3 (0001) substrate at 770 ºC [36] and Cr_2GeC(103) on Al_2O_3 (0001) and MgO (111) substrate at 800 ºC [12]. By considering Ti_2AlN (103) and (116) planes observed in this work, it can be seen that (103) plane is a common plane detected during the nucleation and growth of these M_2AX phase under non-basal plane growth condition. To understand the reason behind the frequent observation of (103) plane, we evaluated the surface energies of various planes using density functional theory (DFT) which was implemented by Vienna ab initio simulation package (VASP) [37]. The projector augmented waves (PAW) pseudopotentials and the generalized gradient approximation parameterized by Perdew, Burke and Ernzerhof were employed [38,39]. Convergence criteria for energy and force were chosen to be less than 1×10^{-5} eV and 0.01 eV/Å, respectively. The surface energy (σ) was calculated using the following expression:

$$\sigma = \lim_{n\to\infty} \frac{1}{2}(E_{slab}^{n} - nE_{bulk}) \quad (2)$$

where E_{slab}^{n} is total energy of a slab which contains n number of bulk unit, and E_{bulk} is the total energy of the bulk [40,41]. Surface was created by cleaving from the optimized bulk structure and was relaxed by optimizing the atoms in the top layers while keeping the bottom three Ti_2AlN atomic planes fixed. The derived surface energies are listed in Table 1 (in ascending order from top to bottom). It can be seen that the surface energies of (101) and (103) are very close and are the lowest, followed by (002) and the rest.

Table 1 Surface energy (σ, in J/m^2) for various Ti_2AlN planes

Ti_2AlN Planes	Surface Energy (σ, in J/m^2)
(101)	1.99
(103)	2.01
(002)	2.14
(110)	2.21
(100)	2.33
(107)	2.44
(116)	2.50
(104)	2.74
(106)	2.83

At a lower temperature between 600 and 720 ^oC where adatoms are energetically limited to diffuse and re-organize freely on the surface, growth of non-basal planes like Ti_2AlN (101) and (103) planes offer the best option to minimize surface energy. When the temperature was increased further to 750 ^oC and above, the adatoms gain sufficient kinetic energy to diffuse freely on the surfaces and basal plane growth of Ti_2AlN is prevailed since Ti_2AlN (0002) plane only has 0.57 % lattice mismatch with MgO (111) plane and also offer relatively low surface energy. Ti_2AlN (101) plane is observed between 600 and 720 ^oC (Fig. 2) but its intensity is much weaker than that of (103) planes due to its structure factor for XRD. This is consistent with the JCPDS-ICDD standard card of Ti_2AlN (00-018-0070), where intensity of (101) plane is only one-tenth of that of (103) plane. Due to the similar effect caused by the structure factor, Ti_2AlN (100) and (110) planes, although present and detected, are less prominent than (103) and (116) planes due to their lower diffraction peak intensities.

Young's modulus, also known as the tensile modulus or elastic modulus, measures the resistance of a material to elastic (recoverable) deformation under load. A material having a very high Young's modulus is rigid. On an atomic scale, the magnitude of the Young's modulus is a measure of the resistance to separate two adjacent atoms (but before they break apart from each

other) and relates to interatomic bonding forces [42]. A development of the structure from polycrystalline at 600 ºC to single crystalline at 750 ºC does not alter the interatomic bonding in the material and hence does not help to improve the Young's modulus significantly (Fig. 4(a)). On the other hand, the indentation hardness reflects a material's resistance towards a permanent inelastic deformation caused by constant downward impression of a sharp indenter from the top surface, and it is therefore related to the material's microstructure. With an increase in deposition temperature, the thin film structure has evolved from intersecting of multiple planes at 600 ºC, to dominantly (103) planes on (002) planes at 720 ºC and eventually to an ordered, layered stack of single (002) planes parallel to substrate plane at 750 ºC. Intuitively, an ordered stack of planes certainly help a material resist the intrusion/penetration of an indenter from surface compared with a mixture of different orientated planes which intersect each other and have gaps in between. As a result, the hardness increased accordingly from 600 to 750 ºC when the surface order improved (Fig. 4(b)).

~~Lastly, we would like to compare the properties of Ti_2AlN against some common metals and ceramics to demonstrate its hybrid metallic-ceramic property (Table 2). The Young's modulus of single crystalline Ti_2AlN is lower than the Young's modulus of TiN and α-AlN. However, it is significantly higher than those of metals including Al, Ti, Ni, steel and even those of ceramics including ZrO_2, MgO and $MgAl_2O_4$. The hardness value of single crystalline Ti_2AlN is higher than the hardness of single crystalline TiN single crystalline α-AlN, and is also much higher than those of ceramics including ZrO_2, MgO and $MgAl_2O_4$.~~

Lastly, we would like to compare the properties of Ti_2AlN against some common metals and ceramics to demonstrate its hybrid metallic-ceramic property (Table 2). The Young's modulus and hardness of single crystalline Ti_2AlN are not only higher than those of single

crystalline nitrides (TiN and α-AlN), but also much higher than those of metals (including Al, Ti, Ni, steel) and even those of ceramics (including ZrO_2, MgO and $MgAl_2O_4$). On the other hand, the electrical resistivity of the single crystalline Ti_2AlN at 750 ºC measured by four point probe is 64.4 ± 2.1 $\mu\Omega$ cm, which is higher than the value of 39 $\mu\Omega$ cm reported earlier [15] and can be attributed to Al vacancy scattering due to an Al-deficient stoichiometry in our Ti_2AlN thin films. This value is one order higher than those of metals including Al, Ni and steel and is comparable with Ti, but is significantly lower than that of ceramic such as MgO. Hence, it can be seen that Ti_2AlN, as one member of the MAX phase materials, possesses properties of ceramic (stiff and hard in mechanical property) and metal (low electrical resistivity) concurrently, which certainly warrants much more research efforts to further explore its potential technological applications such as wear resistant coatings, diffusion barriers, radiation-tolerant cladding material, etc.

Table 2 Comparison of Young's modulus, hardness and resistivity between metals (Al, Ti, Ni and Fe), nitrides (Ti_2AlN, TiN, AlN) and ceramics (ZrO_2, MgO, $MgAl_2O_4$).

Materials Group	Compound	Young's Modulus (GPa)	Hardness (GPa)	Resistivity ($\mu\Omega$ cm)
Metal	Al (>99.5%)	69 [42]	-	2.78 [42]
	Ti (>99%)	107[42]	-	50 [42]
	Ni (>99%)	207 [42]	-	8.47 [42]
	Steel	207 [42]	-	10 [42]
Nitride	**Ti_2AlN**	**487.1 ± 19.3**	**26.5 ± 1.8**	**64.4 ± 2.1**
	TiN	445 ± 38 ~ 449 ± 28 [43]	20 ± 0.8 ~ 21 ± 1 [43]	-
	α-AlN	369 ~ 379 [44]	16 ~ 18 [44]	-
Ceramic	ZrO_2	152 [42]	20.5 [45]	-
	MgO	207 [42]	8.5 - 9.0 [43]	$>10^{20}$ [42]
	$MgAl_2O_4$	284 [42]	25 [45]	-

5. Conclusion

In summary, the composition, crystalline phase, morphology and mechanical properties of Ti-Al-N thin films deposited by DC magnetron sputtering from Ti_2Al alloy in Ar/N_2 plasma as a function of deposition temperature have been investigated. The Ti-Al-N film was a mixture of metallic Ti, Al and (Ti,Al)N cubic solid solution at 500 ºC. Ti_2AlN MAX phase started to form at 600 ºC, and its crystallinity improved with an increase in substrate temperature until the single crystalline Ti_2AlN MAX phase is formed at 750 ºC. With an improvement in the crystallinity shown by XRD from 600 to 750 ºC, there was a decrease in Al% as shown by *in-situ* XPS from 38.7% at 600 ºC to only 14.8 % at 750 ºC. At the same time, surface morphology evolved from small triangle islands at 600 ºC, to bigger triangle islands at 700 ºC, to equilateral triangles at 720 ºC until hexagonal flat-top islands with terrace structure was developed at 750 ºC. In the same process, the hardness increased from 15.8 ± 2.6 GPa at 600 ºC to 26.5 ± 1.8 GPa at 750 ºC, although the Young's modulus remained roughly constant at 412.5 ± 45.6 GPa. Together with DFT calculation results, our findings show that temperature does play an important role in the nucleation and growth of Ti_2AlN MAX thin film. Low temperature promotes growth of non-basal planes with low surface energies, while high temperature facilitates basal plane growth when adatoms are free to diffuse. Temperature is thus an important growth parameter to be tuned in order to achieve the desired crystallinity of the Ti_2AlN MAX thin films.

- **Acknowledgment**

This project was funded by Science and Engineering Research Council (SERC) and supported by Aerospace Program of A*STAR (Grant No: 112 155 0512).

- **References**

[1] M. W. Barsoum, The $M_{n+1}AX_n$ Phases: A New Class of Solids; Thermodynamically Stable Nanolaminates, Prog. Solid State Chem. 28 (2000) 201-281.
[2] P. Eklund, M. Beckers, U. Jansson, H. Hogberg, L. Hultman, The $M_{n+1}AX_n$ Phases: Materials Science and Thin-film Processing, Thin Solid Films 518 (2010) 1851-1878.
[3] M. Beckers, N. Schell, R. M. S. Martins, A. Mucklich, W. Moller, L. Hultman, Nucleation and Growth of Ti_2AlN Thin Films Deposited by Reactive Magnetron Sputtering Onto MgO(111), J. Appl. Phys. 102 (2007) 074916.
[4] Q. M. Wang, A. F. Renteria, O. Schroeter, R. Mykhaylonka, C. Leyens, W. Garkas, M. to Baben, Fabrication and Oxidation Behavior of Cr_2AlC Coating on Ti6242 Alloy, Surf. Coat. Technol. 204 (2010) 2343-2352.
[5] E. N. Hoffman, D. W. Vinson, R. L. Sindelar, D. J. Tallman, G. Kohse, M. W. Barsoum, MAX Phase Carbides and Nitrides: Properties for Future Nuclear Power Plant In-core Applications and Neutron Transmutation Analysis, Nucl. Eng. Des. 244 (2012) 17-24.
[6] K. Buchholt, R. Ghandi, M. Domeij, C.-M. Zetterling, J. Lu, P. Eklund, L. Hultman, A. L. Spetz, Ohmic contact properties of magnetron sputtered Ti_3SiC_2 on n- and p-type 4H-silicon carbide, Appl. Phys. Lett. 98 (2011) 042108.
[7] J. Emmerlich, H. Hogberg, S. Sasvari, P. O. A. Persson, L. Hultman, J. P. Palmquist, U. Jansson, J. M. Molina-Aldareguia, Z. Czigany, Growth of Ti_3SiC_2 Thin Films by Elemental Target Magnetron Sputtering, J. Appl. Phys. 96 (2004) 4817-4826.
[8] P. Eklund, M. Beckers, J. Frodelius, H. Hogberg, L. Hultman, Magnetron Sputtering of Ti_3SiC_2 Thin Films Fom A Compound Target, J. Vac. Sci. Technol.,A 25 (2007) 1381-1388.
[9] J. Frodelius, P. Eklund, M. Beckers, P. O. A. Persson, H. Hogberg, L. Hultman, Sputter Deposition from a Ti_2AlC Target: Process Characterization and Conditions for Growth of Ti_2AlC, Thin Solid Films 518 (2010) 1621-1626.
[10] C. Walter, D. P. Sigumonrong, T. El-Raghy, J. M. Schneider, Towards Large Area Deposition of Cr_2AlC on Steel, Thin Solid Films 515 (2006) 389-393.
[11] J. J. Li, L. F. Hu, F. Z. Li, M. S. Li, Y. C. Zhou, Variation of Microstructure and Composition of the Cr_2AlC Coating Prepared by Sputtering at 370 and 500°C, Surf. Coat. Technol. 204 (2010) 3838-3845.
[12] P. Eklund, M. Bugnet, V. Mauchamp, S. Dubois, C. Tromas, J. Jensen, L. Piraux, L. Gence, M. Jaouen, T. Cabioc'h, Epitaxial Growth and Electrical Transport Properties of Cr_2GeC Thin Films, Phys. Rev. B 84 (2011) 075424.
[13] J. Emmerlich, P. Eklund, D. Rittrich, H. Hogberg, L. Hultman, Electrical Resistivity of $Ti_{n+1}AC_n$ (A = Si, Ge, Sn, n=1-3) Thin Films, J. Mater. Res. 22 (2007) 2279-2287.
[14] O. Wilhelmsson, P. Eklund, H. Hogberg, L. Hultman, U. Jansson, Structural, Electrical and Mechanical Characterization of Magnetron-sputtered V-Ge-C Thin Films, Acta Mater. 56 (2008) 2563-2569.
[15] T. Joelsson, A. Horling, J. Birch, L. Hultman, Single-crystal Ti_2AlN Thin Films, Appl. Phys. Lett. 86 (2005) 111913.
[16] M. Beckers, N. Schell, R. M. S. Martins, A. Mucklich, W. Moller, Phase Stability of Epitaxially Grown Ti_2AlN Thin Films, Appl. Phys. Lett. 89 (2006) 074101.

[17] M. Beckers, N. Schell, R. M. S. Martins, A. Mucklich, W. Moller, L. Hultman, Microstructure and Nonbasal-plane Growth of Epitaxial Ti_2AlN Thin Films, J. Appl. Phys. 99 (2006) 034902.
[18] T. Joelsson, A. Flink, J. Birch, L. Hultman, Deposition of Single-crystal Ti_2AlN Thin Films by Reactive Magnetron Sputtering from a 2Ti : Al Compound Target, J. Appl. Phys. 102 (2007) 074918.
[19] P. O. A. Persson, S. Kodambaka, I. Petrov, L. Hultman, Epitaxial $Ti_2AlN(0001)$ Thin Film Deposition by Dual-target Reactive Magnetron Sputtering, Acta Mater. 55 (2007) 4401-4407.
[20] Z. Zhang, Y. Nie, L. Shen, J. Chai, J. Pan, L. M. Wong, M. B. Sullivan, H. Jin, S. J. Wang, Charge Distribution in the Single Crystalline Ti_2AlN Thin Films Grown on MgO(111) Substrates, J. Phys. Chem. C 117 (2013) 11656-11662.
[21] M. Beckers, C. Höglund, C. Baehtz, R. M. S. Martins, P. O. Å. Persson, L. Hultman, W. Möller, The Influence of Substrate Temperature and Al Mobility on the Microstructural Evolution of Magnetron Sputtered Ternary Ti–Al–N Thin Films, J. Appl. Phys. 106 (2009) 064915.
[22] N. J. Lane, S. C. Vogel, M. W. Barsoum, Temperature-Dependent Crystal Structures of Ti_2AlN and Cr_2GeC as Determined from High Temperature Neutron Diffraction, J. Am. Ceram. Soc. 94 (2011) 3473-3479.
[23] B. N. Lucas, W. C. Oliver, J. E. Swindeman, The Dynamics of Frequency-Specific, Depth-Sensing Indentation Testing, Mater. Res. Soc. Symp. Proc. 522 (1998) 3-14.
[24] I. Milošv, H. H. Strehblow, B. Navinšek, M. Metikoš-Huković, Electrochemical and thermal oxidation of TiN coatings studied by XPS, Surf. Interface Anal. 23 (1995) 529-539.
[25] J. F. Moulder, W. F. Stickle, P. E. Sobol, K. D. Bomben. Handbook of X-ray Photoelectron Spectroscopy: A Reference Book of Standard Spectra for Identification and Interpretation of XPS Data. 6509 Flying Cloud Drive, Eden Prairie, Minnesota 55344, United States of America: Physical Electronics, Inc., 1995.
[26] I. Bertoti, Characterization of Nitride Coatings by XPS, Surf. Coat. Technol. 151 (2001) 194-203.
[27] D. E. Mencer, T. R. Hess, T. Mebrahtu, D. L. Cocke, D. G. Naugle, Surface Reactivity of Titanium Aluminum-Alloys - Ti_3Al, TiAl, and $TiAl_3$, J. Vac. Sci. Technol. A 9 (1991) 1610-1615.
[28] V. Dolique, M. Jaouen, T. Cabioc’h, F. Pailloux, P. Guérin, V. Pélosin, Formation of (Ti,Al)N／Ti_2AlN Multilayers After Annealing of TiN／TiAl(N) Multilayers Deposited by Ion Beam Sputtering, J. Appl. Phys. 103 (2008) 083527.
[29] T. Zhang, H. B. Myoung, D. W. Shin, K. H. Kim, Syntheses and Properties of Ti_2AlN MAX-phase Films, J. Ceram. Process. Res. 13 (2012) S149-S153.
[30] Z. Zhang, H. Jin, J. Pan, J. Chai, L. M. Wong, M. B. Sullivan, S. J. Wang, Origin of Al Deficient Ti_2AlN and Pathways of Vacancy-Assisted Diffusion, J. Phys. Chem. C 119 (2015) 16606-16613.
[31] J. Y. Wang, Y. C. Zhou, T. Liao, J. Zhang, Z. J. Lin, A First-principles Investigation of the Phase Stability of Ti_2AlC with Al Vacancies, Scr. Mater. 58 (2008) 227-230.
[32] J. Xiao, T. Yang, C. Wang, J. Xue, Y. Wang, Investigations on Radiation Tolerance of $M_{n+1}AX_n$ Phases: Study of Ti_3SiC_2, Ti_3AlC_2, Cr_2AlC, Cr_2GeC, Ti_2AlC, and Ti_2AlN, J. Am. Ceram. Soc. 98 (2015) 1323-1331.
[33] M. Bugnet, T. Cabioc'h, V. Mauchamp, P. Guerin, M. Marteau, M. Jaouen, Stability of the Nitrogen-deficient Ti_2AlN_x MAX Phase in Ar^{2+}-irradiated (Ti,Al)N/Ti_2AlN_x Multilayers, J. Mater. Sci. 45 (2010) 5547-5552.

[34] D. J. Tallman, E. N. Hoffman, E. a. N. Caspi, B. L. Garcia-Diaz, G. Kohse, R. L. Sindelar, M. W. Barsoum, Effect of Neutron Irradiation on Select MAX Phases, Acta Mater. 85 (2015) 132-143.
[35] Z. Zhang, H. Jin, J. Chai, L. Shen, H. L. Seng, J. Pan, L. M. Wong, M. B. Sullivan, S. J. Wang, Desorption of Al and Phase Transformation of Ti_2AlN MAX Thin Film upon Annealing in Ultra-High-Vacuum, J. Phys. Chem. C 118 (2014) 20927-20939.
[36] J. Frodelius, J. Lu, J. Jensen, D. Paul, L. Hultman, P. Eklund, Phase Stability and Initial Low-Temperature Oxidation Mechanism Of Ti_2AlC Thin Films, J. Eur. Ceram. Soc. 33 (2013) 375-382.
[37] G. Kresse, J. Hafner, Ab-Initio Molecular-Dynamics Simulation of the Liquid-Metal Amorphous-Semiconductor Transition in Germanium, Phys. Rev. B 49 (1994) 14251-14269.
[38] P. E. Blochl, Projector Augmented-Wave Method, Phys. Rev. B 50 (1994) 17953-17979.
[39] J. P. Perdew, K. Burke, M. Ernzerhof, Generalized Gradient Approximation Made Simple, Phys. Rev. Lett. 77 (1996) 3865-3868.
[40] N. E. Singh-Miller, N. Marzari, Surface Energies, Work Functions, and Surface Relaxations of Low-Index Metallic Surfaces from First Principles, Phys. Rev. B 80 (2009) 235407.
[41] J. L. F. Da Silva, C. Stampfl, M. Scheffler, Converged Properties of Clean Metal Surfaces by All-Electron First-Principles Calculations, Surf. Sci. 600 (2006) 703-715.
[42] W. D. Callister. Materials Science and Engineering : An Introduction. Hoboken, NJ John Wiley & Sons, 2007.
[43] H. Ljungcrantz, M. Oden, L. Hultman, J. E. Greene, J. E. Sundgren, Nanoindentation Studies of Single-crystal (001)-, (011)-, and (111)-oriented TiN Layers on MgO, J. Appl. Phys. 80 (1996) 6725-6733.
[44] I. Yonenaga, T. Shima, M. H. F. Sluiter, Nano-Indentation Hardness and Elastic Moduli of Bulk Single-Crystal AlN, Jpn. J. Appl. Phys., Part 1 41 (2002) 4620-4621.
[45] K. E. Sickafus, C. J. Wetteland, N. P. Baker, N. Yu, R. Devanathan, M. Nastasi, N. Bordes, A Comparison Between the Irradiation Damage Response of Spinel And Zirconia Due to Xe Ion Bombardment, Mater. Sci. Eng., A 253 (1998) 78-85.

List of Figures Captions

Fig.1 High resolution XPS spectra of (a) Ti 2p, (b) Al 2p, (c) N 1s, (d) valence band (VB) and (e) Mg 1s and O 1s captured at various deposition temperatures of 500, 600, 700, 720 and 750 ^{o}C. The spectra in each figure are normalized to have the same maximum peak heights with the scaling factor indicated near the left axis of each spectrum for easy comparison. The resulting composition of the respective Ti-Al-N thin film after deposition is calculated based on the corresponding peak areas from panels (a)-(c) and is shown in panel (f).

Fig.2 The first frame covering the X-ray diffraction patterns in the 2θ range from 10 to 46^{o} captured by the general area detector for the Ti-Al-N thin films deposited at (a) 500, (b) 600, (c) 700, (d) 720 and (e) 750 ^{o}C. (f) shows the XRD patterns from the Ti-Al-N thin film deposited from 500 to 750 ^{o}C after integrating the respective two frames of XRD diffraction patterns.

Fig.3 Column (i) 5 × 5 μm^2 (left panel) and (ii) 2 × 2 μm^2 (right panel) AFM images of the Ti-Al-N thin films deposited (a) 500, (b) 600, (c) 700, (d) 720 and (e) 750 ^{o}C. Blue circle in (b, ii) highlights an island having a triangle shape, while black circles in (d, i) mark flat areas on top of which the islands grow.

Fig.4 (a) Young's modulus and (b) hardness of the Ti-Al-N thin films deposited from 500 to 750 ^{o}C as measured by nano-indentation.

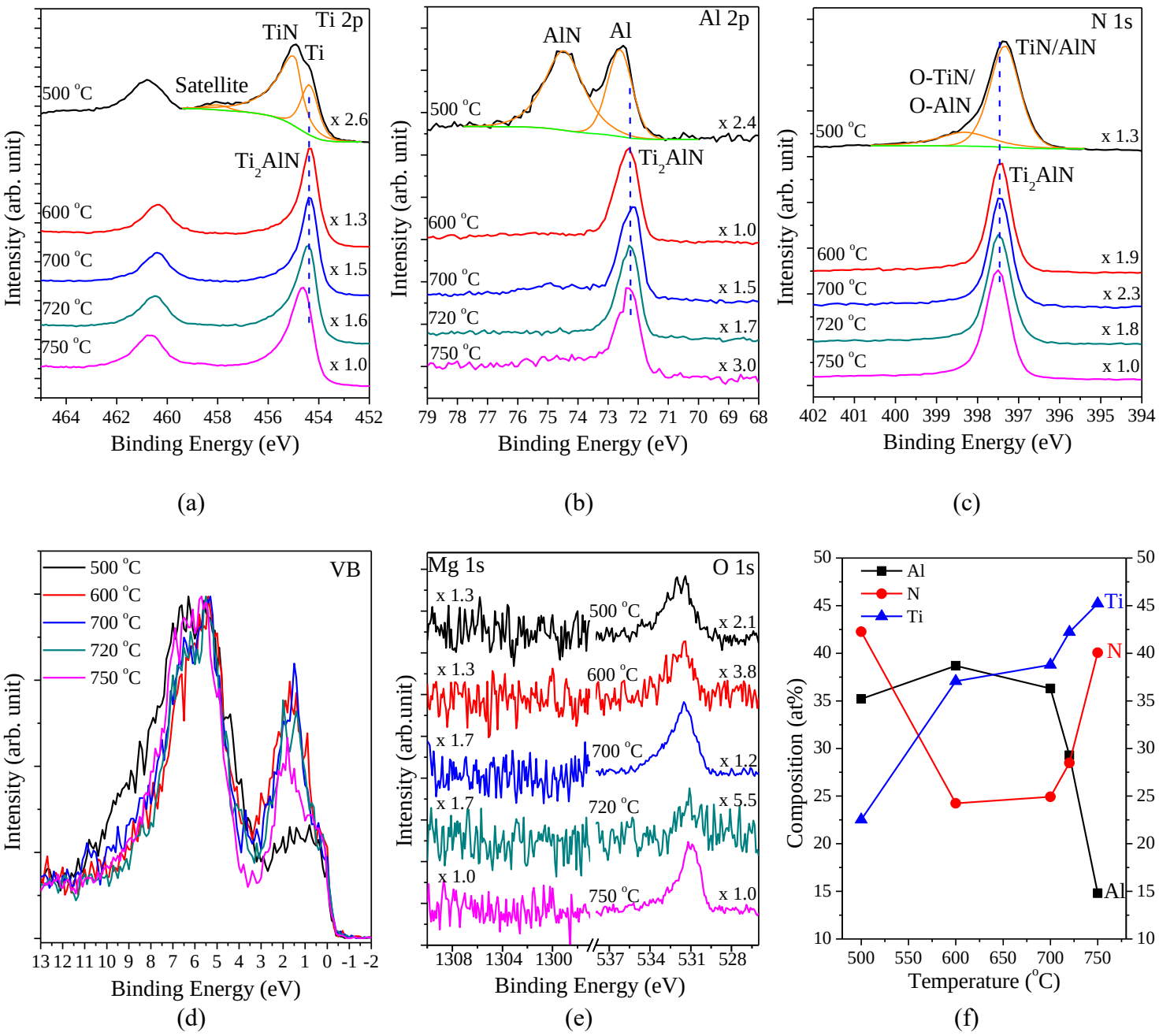

Figure 1. Zhang *et al*.

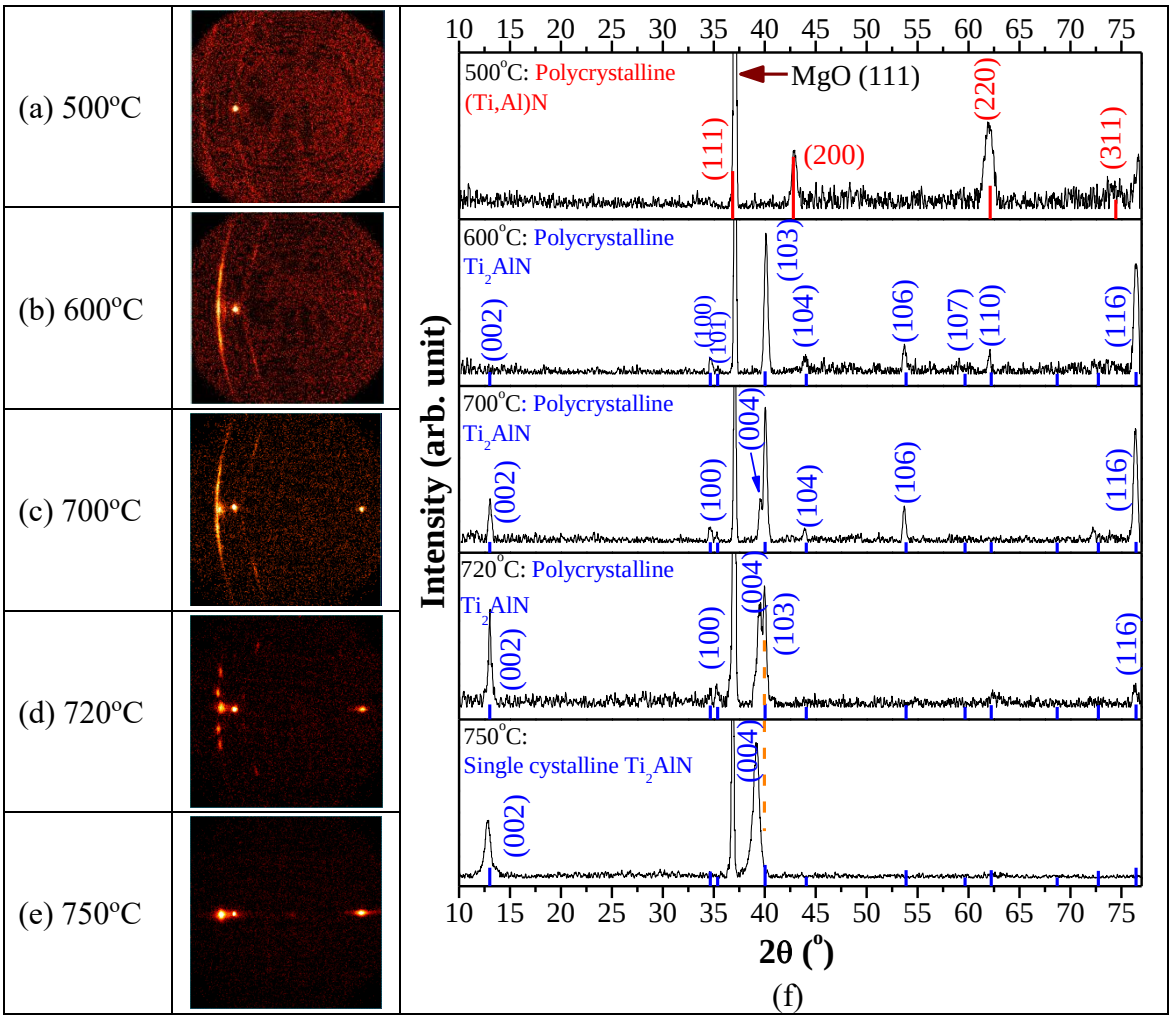

Figure 2. Zhang *et al*.

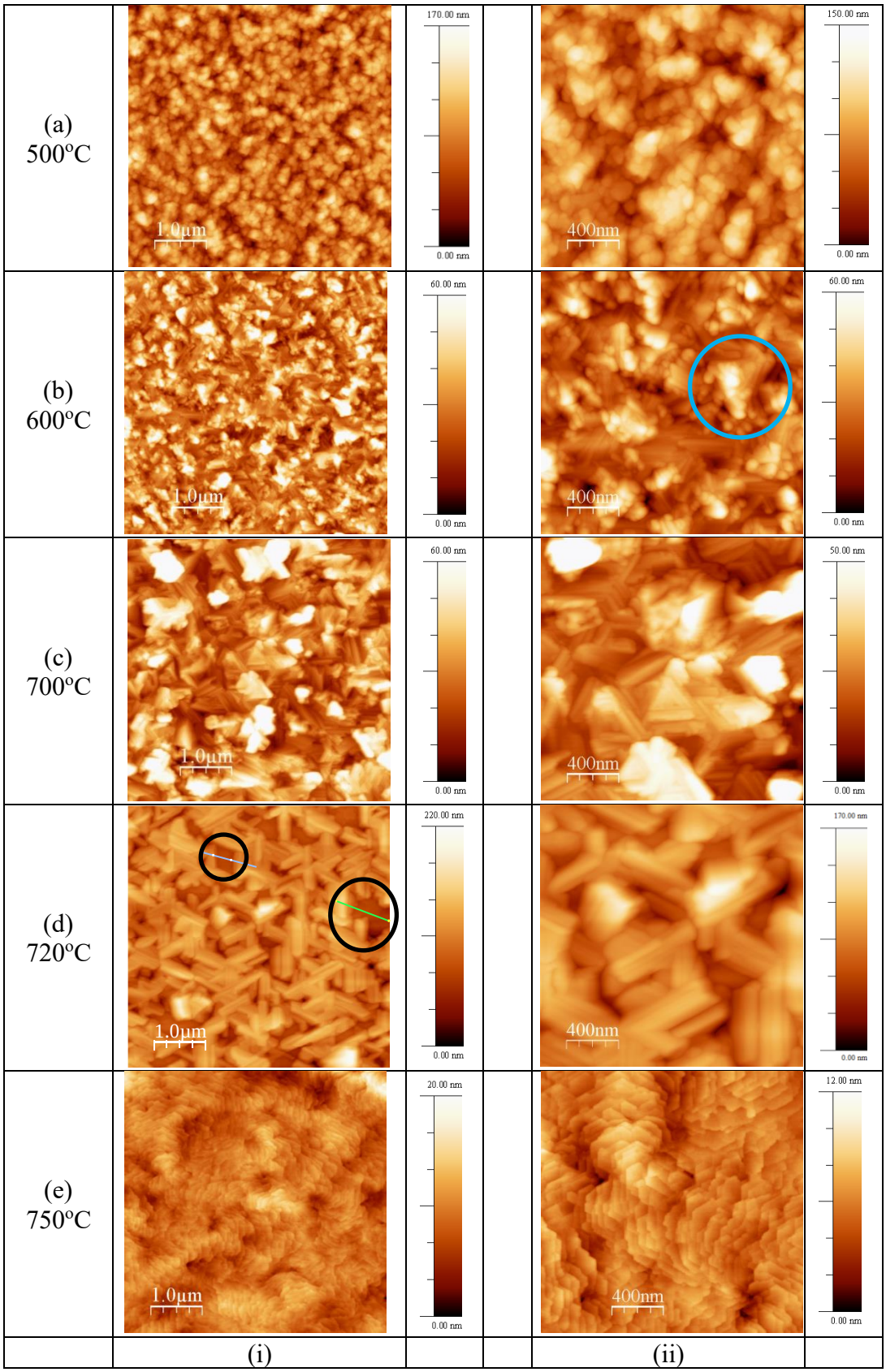

Figure 3. Zhang *et al*.

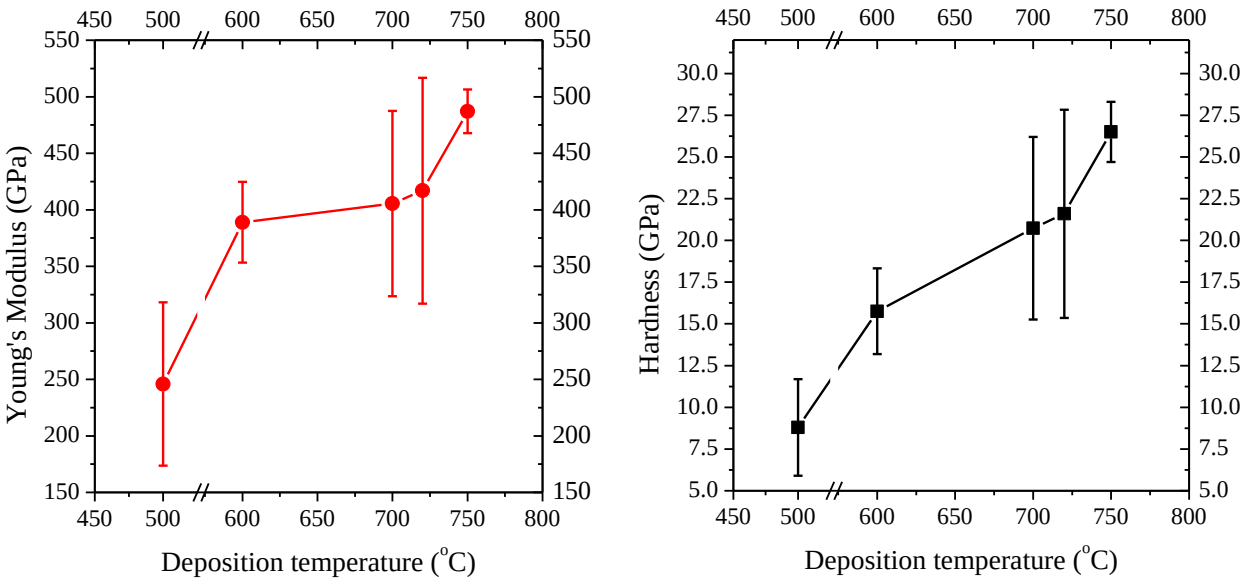

(a) (b)

Figure 4. Zhang *et al*.